Journal of Materials Science and Engineering with Advanced Technology
Volume 5, Number 1, 2012, Pages 39-70

INFLUENCE OF STEP-DOWN AUSTEMPERING PROCESS ON THE FRACTURE TOUGHNESS OF AUSTEMPERED DUCTILE IRON

SUSIL K. PUTATUNDA and GOWTHAM A. BINGI

Department of Chemical Engineering and Materials Science
Wayne State University
Detroit, MI 48202
USA
e-mail: sputa@eng.wayne.edu

Abstract

Austempered ductile cast iron (ADI) has emerged as a major engineering material in recent years because of its many attractive properties. In this investigation, the influence of a step-down austempering process on the microstructure and mechanical properties including fracture toughness of an unalloyed ductile cast iron was examined. Compact tension and cylindrical tensile specimens were prepared from unalloyed nodular cast iron as per ASTM standards and were subjected to conventional as well as step-down austempering process at three different austempering temperatures. The microstructure and mechanical properties of these samples were evaluated and compared.

Test results show that both the step-down and conventional austempering process resulted in very similar microstructure and mechanical properties in unalloyed ADI. The fracture toughness of the material was found to be influenced by both ferritic cell size (d) and the austenitic carbon $(X_\gamma.C_\gamma)$.

Keywords and phrases: ferrite, austenite, austempered ductile cast iron (ADI), fracture toughness, microstructure, step-down, mechanical properties.

Received October 7, 2011

1. Introduction

Austempered ductile cast iron (ADI) has emerged as a major engineering material in recent years. It is produced by austempering of nodular or ductile cast iron in the temperature range of 260°C-400°C. This heat treatment produces a unique microstructure consisting of acicular ferrite (α) and carbon stabilized austenite (γ_{HC}). As a result of this microstructure, ADI develops many attractive mechanical properties, such as high strength with good ductility [9, 13, 14, 20], good fatigue strength [4, 5, 7, 21, 35, 38], high fracture toughness [10, 22, 23, 25, 28-30, 37], and good wear resistance [16, 34, 39].

ADI also has several advantages over steel and aluminum as a structural material. For example, because of its lower density than steel, it has higher specific strength compared to conventional quenched and tempered steels [18]. Moreover, because of the presence of graphite nodules, its machinability is also higher than steel [17] and it has a better damping capacity. Although it is heavier than aluminum, ADI has three times the strength and twice the stiffness of aluminum [31]. Because of these attractive properties, ADI is widely used now-a-days in many engineering applications, such as automotive, agricultural, construction, and mining components etc..

During austempering, a two-stage phase transformation occurs in ADI. In the first stage, the austenite (γ) decomposes into ferrite (α) and high-carbon austenite (γ_{HC}).

$$\gamma \longrightarrow \alpha + \gamma_{HC}. \tag{1}$$

If the alloy is held at the austempering temperature for too long (beyond the process window), the high carbon austenite (γ_{HC}) can further decompose into ferrite (α) and carbide (ε). As a result of this reaction, the material becomes embrittled and thereby loses its ductility and toughness. Therefore, for successful production of ADI, the alloy

must be austempered within the process window. The process window is defined as the time interval between the completion of first reaction and the onset of the second (embrittlement) reaction. The alloying elements such as nickel and molybdenum are generally added to conventional ADI to enlarge this process window. Therefore, conventional ADI usually has some nickel (1.5%) and molybdenum (0.3%) in it. The microstructure of ADI depends on austempering temperature and time, the important microstructural features are the morphology of the phases, i.e., ferrite and austenite, carbon content of austenite, and the presence or absence of undesirable phases such as carbides, pearlites, and martensites.

The austempering reaction in ADI is a nucleation and growth process [12, 19]. During austempering, the ferrite nucleates out of austenite and then grows into the surrounding austenite. As the ferrite grows, the austenite becomes more and more enriched with carbon and as a result, the M_S (martensite start) temperature of the material decreases and austenite becomes more stable. At lower austempering temperature, the ferrite and austenite becomes finer and has the appearance of a lower bainitic structure. On the other hand, at higher austempering temperature, the ferrite and austenite has a feathery appearance of a upper bainitic structure.

The conventional austempering process of ADI involves first austenitizing the alloyed nodular cast iron in the temperature range of 815°C-927°C (1500°F-1700°F) for about 2 hours till the structure becomes fully austenitic. After that, the alloy is quenched in a molten salt bath to a lower temperature between 260°C-400°C and isothermally held at this temperature for about 2 hours and finally air-cooled. A schematic of the typical conventional austempering process is shown in Figure 1.

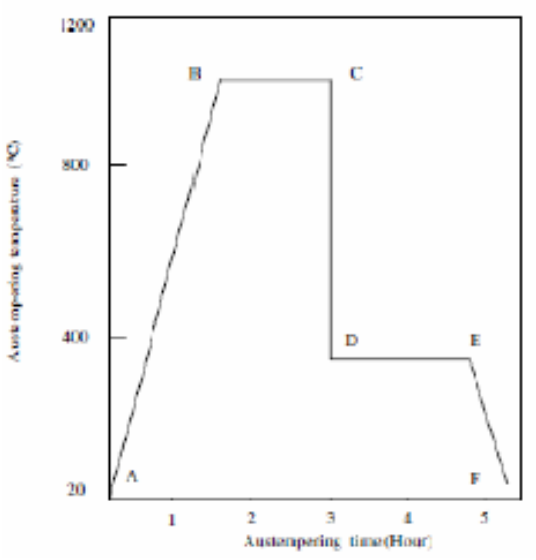

Figure 1. Schematic of conventional austempering process.

In this figure,

A-B: Heat up to the austenitizing temperature.

B-C: Hold at the austenitizing temperature (2 hours).

C-D: Quench to the austempering temperature.

D-E: Hold at the austempering temperature.

E-F: Air cool to room temperature.

The mechanical properties of ADI depend on the microstructure, which in-turn depends on the austempering process. In order to obtain a better combination of strength and fracture toughness in ADI at lower processing cost, a step-down austempering process was conceived. In this step-down austempering process, the nodular or ductile cast iron after austenitizing is first quenched into a higher temperature and then immediately after nucleation is complete, the temperature of the salt bath (quenching medium) is reduced. The alloy is held at the second temperature for about 2 hours and finally air-cooled. A schematic of the step-down austempering process is shown in Figure 2.

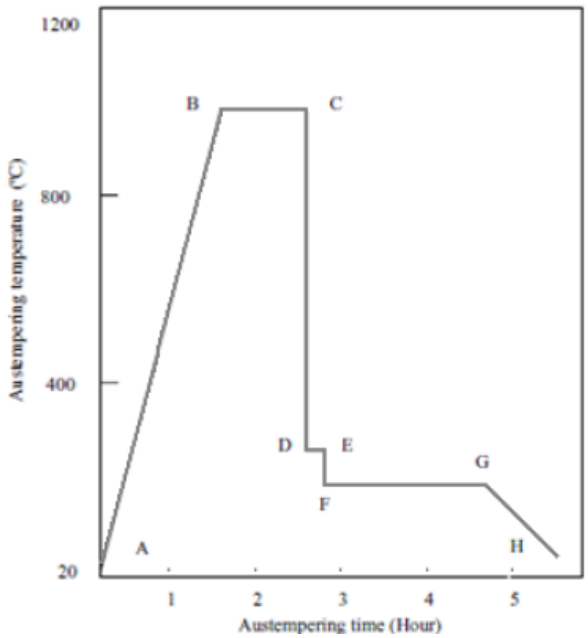

Figure 2. Schematic of the step-down austempering process.

In this figure,

A-B: Heat up to the austenitizing temperature.

B-C: Hold at the austenitizing temperature (2 hours).

C-D: Quench to the first austempering temperature.

D-E: Hold at the first austempering temperature.

E-F: Cool down to the second austempering temperature.

F-G: Hold at the second austempering temperature.

G-H: Air-cool to room temperature.

The present investigation was undertaken to examine whether by employing step-down austempering process, ADI can be produced without compromising any of the mechanical properties. While in a previous investigation [26], the effect of step-down austempering process on the mechanical properties of conventional (alloyed) ADI was examined, in

this investigation, the influence of step-down austempering process on the microstructure and mechanical properties (including fracture toughness) of an unalloyed ADI (without any alloying elements) was studied.

2. Experimental Procedure

2.1. Material

The material used in this investigation was an unalloyed nodular cast iron. The chemical composition of the material is reported in Table 1. The material was cast in the form of KEEL blocks and from these cast blocks, cylindrical tensile test specimens and compact tension specimens for fracture toughness tests were prepared as per ASTM standards E-8 [2] and E-399 [3], respectively.

Table 1. Chemical composition of the material

Element	Percentage (wt%)
C	3.6
Si	2.5
Mn	0.4
S	0.015
P	0.015
Mg	0.010
Cu	0.5
Fe	Balance

2.2. Heat treatment

Two batches of samples were prepared. The first batch of samples (Batch A) was processed by conventional austempering process. These samples were divided into three groups and all the samples were initially austenitized at 927°C (1700°F) for 2 hrs and then subsequently austempered at 288°C (550°F), 316°C (600°F), and 371°C (700°F), respectively, for 2 hrs.

The second batch of samples (Batch B) was processed by step-down austempering process. These samples were also initially austenitized at 927°C (1700°F) for 2 hrs and quenched in a molten salt bath maintained at 288°C (550°F), 316°C (600°F), and 371°C (700°F). After quenching at these temperatures, the temperature of the salt bath was reduced by 28°C (50°F) in 2 hrs in each case and the samples were austempered in the salt bath during this time period. Because of the limitation of the experimental setup at Wayne state, the temperature of the salt bath could be reduced and controlled by 28°C only.

2.3. Tensile testing

Tensile testing of these samples was carried out as per ASTM standard E-8 [2]. The tests were carried out at a constant engineering strain rate of $4 \times 10^{-4} \mathrm{s}^{-1}$ on a servo hydraulic MTS (material test system) test machine at room temperature and ambient atmosphere. Load and displacement plots were obtained on an X-Y recorder and from these load-displacement diagrams, yield strength, ultimate tensile strength, and % elongation values were calculated. Four samples were tested from each heat treated condition and the average values are reported here.

2.4. Fracture toughness testing

After heat treatment, the compact samples were ground and then polished with 600 grit emery paper. The specimens were then pre-cracked in fatigue at ΔK level of 10MPa$\sqrt{\mathrm{m}}$ with a load ratio R = 0.10 to produce a 2mm sharp crack-front in accordance with the ASTM standard E-399 [3]. After fatigue pre-cracking, the specimens were loaded in tension in a servo-hydraulic MTS test machine and the load-displacement diagrams were obtained with a clip-gauge in the knife edge attachment on the specimens. From these load displacement diagrams, P_Q values were determined by using the 5% secant deviation technique as per ASTM standard E-399 [3]. From these P_Q values, K_Q values were determined

by using the standard stress intensity factor calibration function for the compact tension specimens. Since these K_Q values satisfied all the requirements for a valid K_{IC} test as per ASTM standard E-399, they are all valid K_{IC} values.

2.5. Metallography and X-ray diffraction studies

Microstructures of all the samples were examined by optical microscopy after polishing and etching with 5% nital solution. X-ray diffraction (XRD) analysis was performed to estimate the austenite content and the carbon content of austenite following the procedure of Rundman and Klug [33]. XRD was done by using a monochromatic copper K_α radiation at 40kV and 100mA. A Rigaku rotating head anode diffractometer was used to scan angular 2θ range from 42^o-46^o at a scanning speed of 0.25^o per minute and in 2θ range of 72^o-92^o at a scanning speed of 1^o per minute. The profiles were analyzed by using Jade 5 software to obtain the peak positions and the integrated intensities of {111}, {220}, and {311} planes of FCC austenite and {110} and {211} planes of BCC ferrite. The volume fractions of ferrite (X_α) and austenite (X_γ) were determined by the direct comparison method by using the integrated intensities of the above planes [8]. The carbon content of the austenite was determined by the equation [32]

$$a_\gamma = 0.3548 + 0.00441C_\gamma, \tag{2}$$

where a_γ is the lattice parameter of austenite in nanometer and C_γ is the carbon content of austenite in wt%. The {111}, {220}, and {311} planes of austenite were used to estimate the lattice parameter. Two to three samples were examined from each heat treated condition and the data reported is the average from these samples.

3. Results and Discussion

3.1. Influence of austempering temperature on the microstructure

The microstructure of the as-cast sample is reported in the Figure 3. It shows a predominantly pearlitic structure with graphite nodules dispersed in it. The graphic nodules were well rounded with nodularity of about 85%. The microstructures of the conventionally heat treated samples are reported in Figures 4(a), 4(b), and 4(c), respectively, while the microstructure of the samples processed by step-down austempering process are reported in Figures 5(a), 5(b), and 5(c). The microstructure of all these samples (both conventionally austempered as well as processed by step-down austempering process) show a mixture of bainitic ferrite and austenite. The ferrite appears as dark needles, where as austenite appears as white in the microstructure. The austenite has the appearance of slivers between finite needles. It also apparent that both the ferrite and austenite coarsen as the austempering temperature is increased.

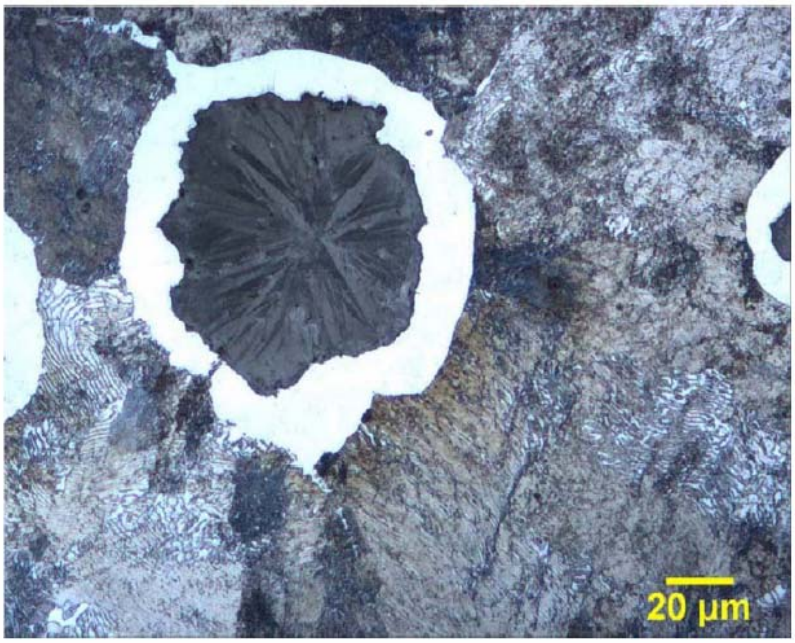

Figure 3. Microstructure of the as-cast iron.

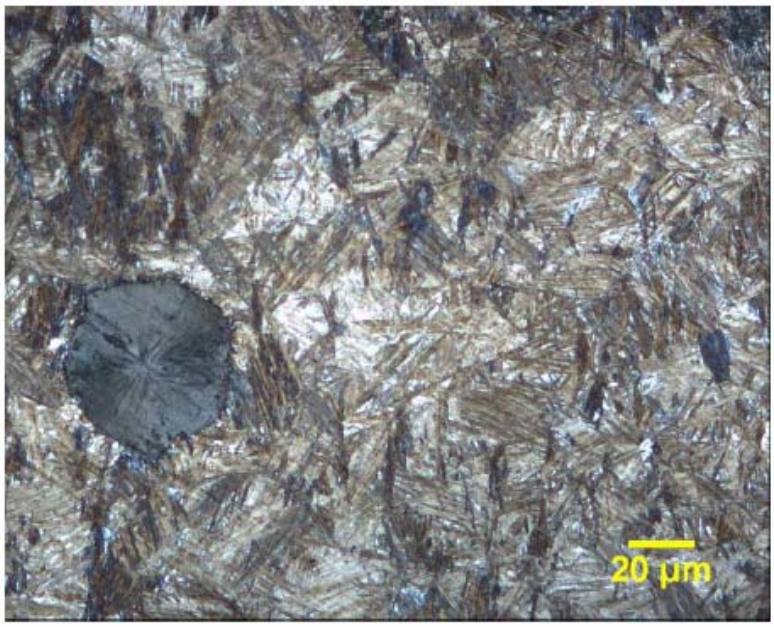

(a)

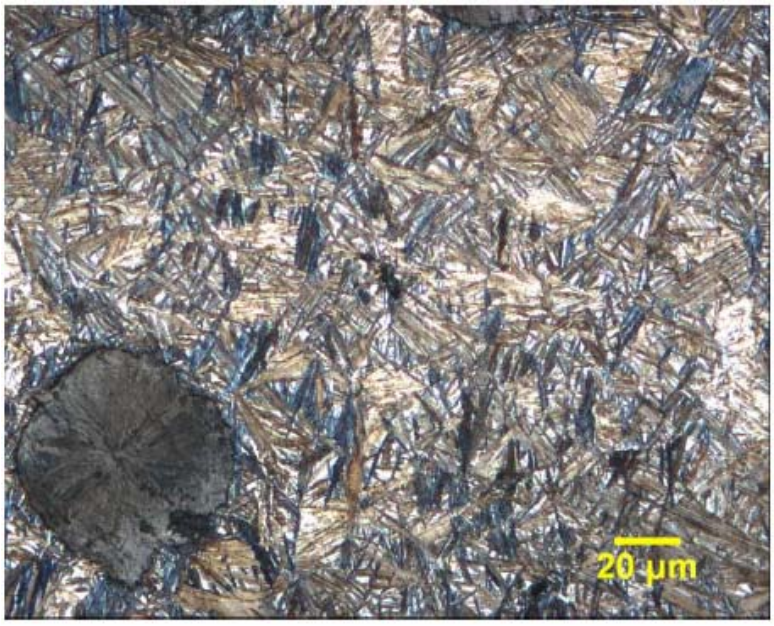

(b)

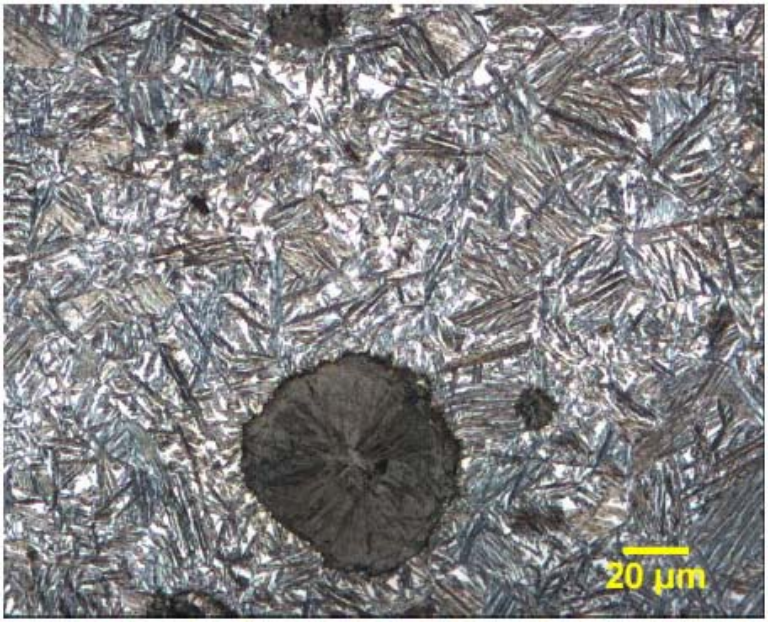

(c)

Figure 4. Microstructures of ADI heat-treated by conventional austempering process. All samples were austenitized at 927°C (1700°F) for 2h and austempered in salt bath maintained at: (a) 288°C (550°F); (b) 316°C (600°F); and (c) 371°C (700°F). Samples were etched by 5% nital, 500X.

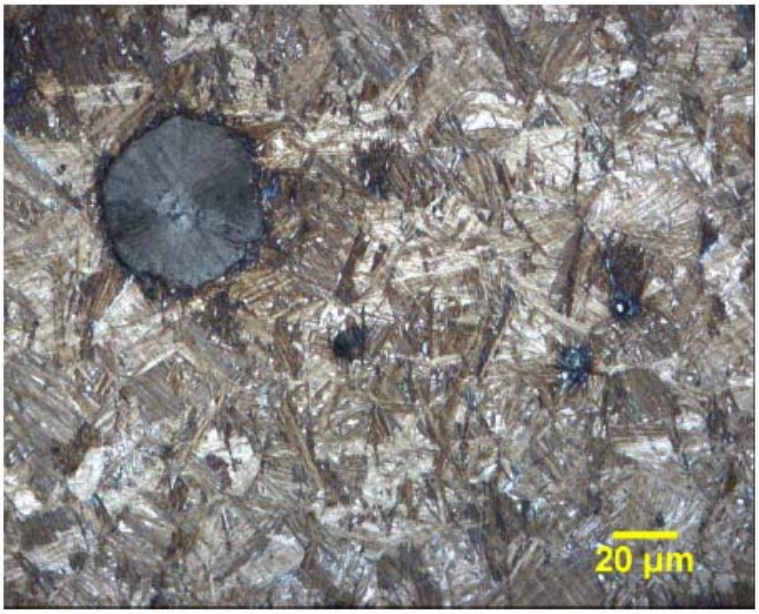

(a)

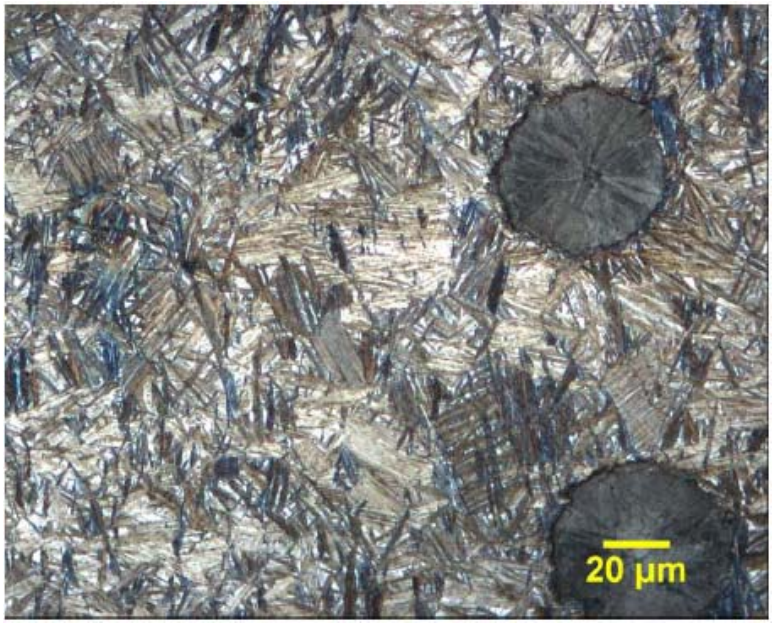

(b)

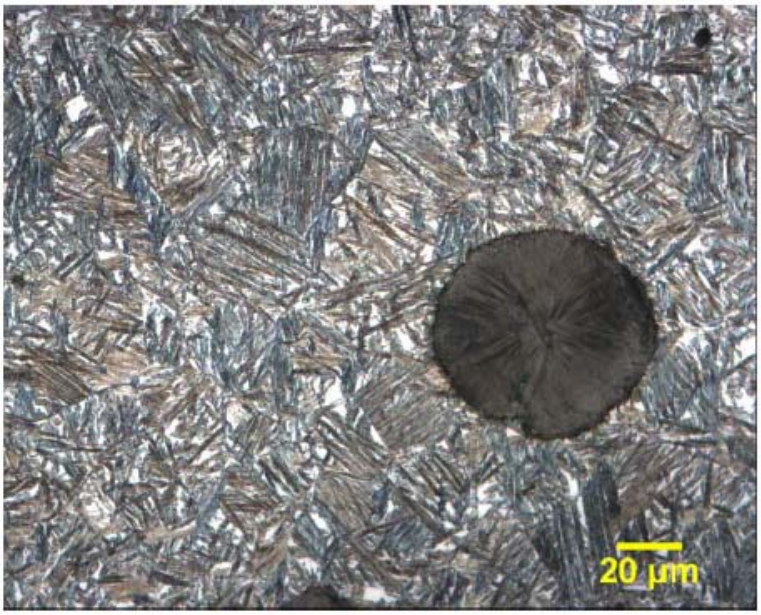

(c)

Figure 5. Microstructures of ADI heat-treated by step-down austempering process. All samples were austenitized at 927ºC (1700ºF) for 2h and austempered in salt bath maintained at: (a) 288ºC-260ºC (550ºF-500ºF); (b) 316ºC-288ºC (600ºF-550ºF); and (c) 371ºC-343ºC (700ºF-650ºF). Samples were etched by 5% nital, 500X.

The ferritic cell size (d) was determined for all these samples by using the well known Scherrer equation [8]. This is also a measure of the mean free path for the dislocation motion. Figure 6 is a plot of the ferritic cell size against austempering temperature. This figure shows that the ferritic cell size (d) increases as the austempering temperature increases, confirming the fact that the ferrite coarsens at higher austempering temperatures. No significant difference was observed in ferritic needle sizes between step-down and conventional austempering process. During austempering process, ferrite first nucleates out of austenite by the nucleation process and then grows with austempering time. As the ferrite grows, the remaining austenite also grows in size. The nucleation process depends on the supercooling (ΔT) and is almost instantaneous. In case of

both step-down and conventional austempering process, the specimens were quenched to the same initial austempering temperatures and hence the supercooling (ΔT) was the same. However, in the step-down austempering process, the temperature of the salt bath was further reduced by 28°C in two hours. It appears that this decrease in temperature was not sufficient enough to significantly affect the growth rate of the ferrite needles and as a result, both step-down and conventional austempering process has resulted in very similar sized ferritic needles.

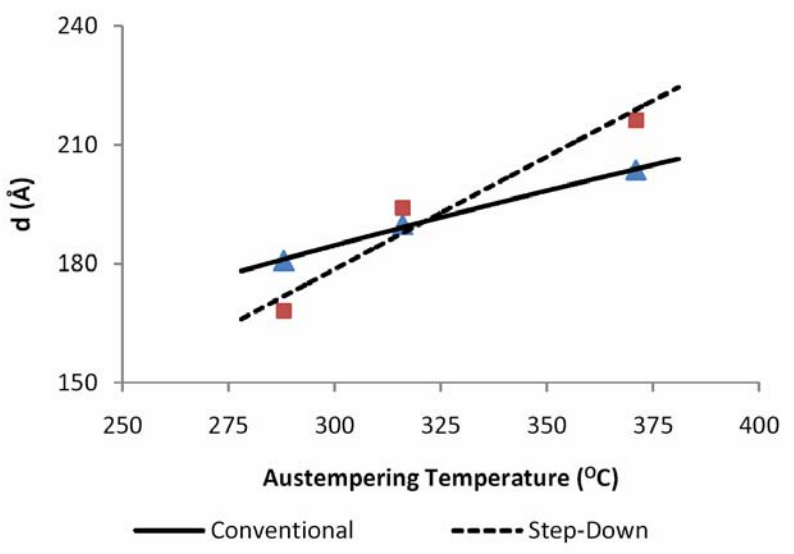

Figure 6. A plot of ferritic cell size vs. austempering temperature.

Table 2 reports the effect of austempering temperature on the volume fraction of ferrite (X_α) of both conventional and step-down austempering process. Both step-down and conventional austempering process have resulted in very similar volume fractions of ferrite at the same austempering temperatures. It is also evident from this table that, the ferrite content decreases as the austempering temperature increases. This can be attributed to the nature of the phase transformation kinetics, i.e., nucleation and growth. At higher austempering temperature (e.g., 371°C), supercooling (ΔT) (difference between austenitizing temperature and austempering temperature) is lower, at the same time, the growth

rate is higher. This causes reduction in nucleation rate of ferrite and consequently fewer ferrite needles grow to a larger size. The ultimate effect is lower volume fraction of ferrite at higher austempering temperatures with coarser appearance. On the other hand, at lower austempering temperature, i.e., 288°C, the supercooling (ΔT) is larger, but the growth rate of ferrite is lower. Consequently, the nucleation rate of ferrite is more and this causes a very large number of ferrite needles to grow to a smaller size and this leads to larger volume fraction of ferrite with finer needles at lower austempering temperature. This also indicates that the volume fraction of austenite will increase with the increase in austempering temperature.

Table 2. Effect of austempering temperature on volume fraction of ferrite

Austempering temperature (°C)	Volume fraction of ferrite (%)
288 Conventional	91.6
288 Step-down	91.0
316 Conventional	85.4
288 Step-down	88.8
371 Conventional	80.6
288 Step-down	81.9

It has been found to be so as shown in Figure 7, where the volume fraction of austenite (X_γ) has been plotted against austempering temperature. It is evident that as the austempering temperature increases, the volume fraction of austenite also increases. Again no significant difference was observed between the austenitic content of the step-down and conventional austempering process at the same austempering temperature. On closer examination of the microstructure, some untransformed austenite (γ) was observed in the material. The untransformed austenite (γ) content was higher in the samples processed by step-down austempering process.

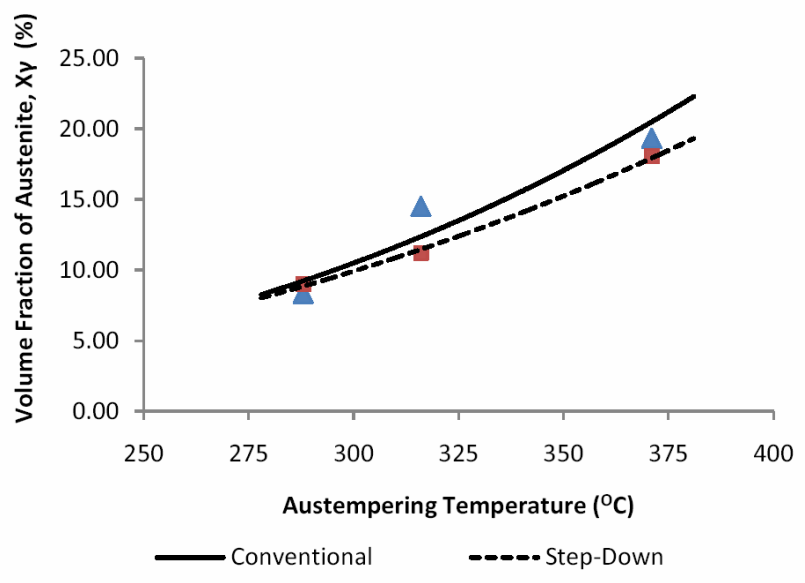

Figure 7. A plot of retained austenite content vs. austempering temperature.

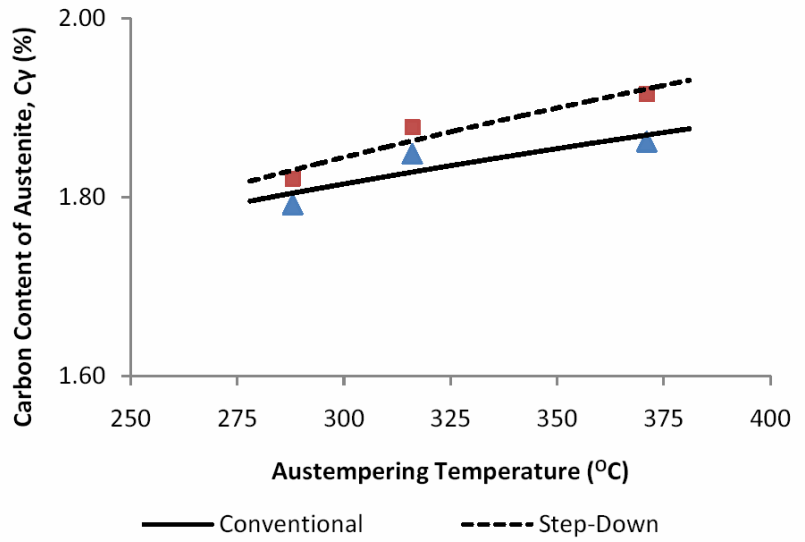

Figure 8. A plot of carbon content of austenite vs. austempering temperature.

Figure 8 is a plot of carbon content of austenite against austempering temperature. It is evident that the carbon content of austenite increases as the austempering temperature increases. As the ferrite needles grow during austempering process, the remaining austenite absorbs more and more carbon and hence the carbon content of the austenite increases with the increase in austempering temperatures. However, no significant difference was observed between the carbon content of austenite in step-down and conventional process.

The carbon content of the parent austenite (C_0) at the austenitizing temperature is fixed and can be obtained by the following equation [36]:

$$C_0 = T_\gamma / 420 - 0.17(\%\mathrm{Si}) - 0.95, \tag{3}$$

where T_γ is the austenitizing temperature in °C.

This carbon (C_0) will be distributed between the ferrite and austenite. Therefore,

$$C_0 = X_\alpha.C_\alpha + X_\gamma.C_\gamma, \tag{4}$$

where X_α is the volume fraction of ferrite, C_α is the carbon content of ferrite, X_γ is the volume fraction of austenite, and C_γ is the carbon content of austenite.

Now ferrite dissolves very little carbon $(C_\alpha \approx 0.002)$ therefore, it can be approximated

$$C_0 = X_\gamma.C_\gamma. \tag{5}$$

Since C_0 is fixed and in the present case ≈ 0.825, most of this carbon will be distributed in the austenite. Table 3 reports the austenitic carbon content $(X_\gamma.C_\gamma)$ as a function of austempering temperature. This product value $X_\gamma.C_\gamma$ is less than C_0 as evident from Table 3. The reason for this difference is due to the fact that at higher austempering temperature, some of the carbon from austenite precipitates in the intercellular region

of the ferrite and austenite leading to the upper bainitic structure. While at lower austempering temperatures, the carbon precipitates within the ferrite needles forming the lower bainitic structures in the ADI.

Table 3. Influence of austempering temperature on austenitic carbon $(X_\gamma.C_\gamma)$

Austempering temperature (°C)	$X_\gamma.C_\gamma$ (conventional)	$X_\gamma.C_\gamma$ (step-down)
288	0.13	0.16
316	0.26	0.21
371	0.35	0.34

The austenitic carbon content $(X_\gamma.C_\gamma)$ is a very important microstructural parameter. This parameter is a measure of the total carbon in the austenite. It is evident that as the austempering temperature increases, the austenitic carbon $(X_\gamma.C_\gamma)$ also increases. This is because both the austenite and the carbon content increases with the austempering temperatures. However, we observe no significant difference in the austenitic carbon content in step-down and conventional austempering process. Thus, it can be concluded that both step-down and conventional austempering process has resulted in very similar microstructure in this unalloyed ductile cast iron and the difference of 28°C (50°F) was not sufficient to affect the growth rate of the ferritic needles and consequently, the volume fraction of austenite and its carbon content.

3.2. Influence of austempering temperature on mechanical properties

Figure 9 reports the effect of austempering temperature on the hardness of the material for both the step-down and conventional austempering process. It is evident that hardness of the material decreases as the austempering temperature increases. However, there was no significant difference in the observed hardness of step-down and

conventional austempering process. Figures 10, 11, and 12 report the effect of austempering temperature on the various mechanical properties of the material such as yield and tensile strength and % elongation for both the step-down and conventional austempering process. Here again, the yield and tensile strengths decrease as the austempering temperature increases; however, the ductility increases at higher austempering temperatures. Again, no significant difference was observed in the tensile strength and % elongation of conventionally processed samples and samples processed by step-down austempering process. The yield strength of the ADI processed by step-down austempering process is slightly higher at lower austempering temperature (288°C) This is apparently be due to the slight difference in ferritic cell size (d) in conventional and step-down austempering process at this temperature. The higher yield strength at lower austempering temperature is because the combined effect of higher ferrite content and smaller ferritic cell size. On the other hand, coarser ferritic cell size and lower ferrite content at higher austempering temperature results in lower yield strength and hardness.

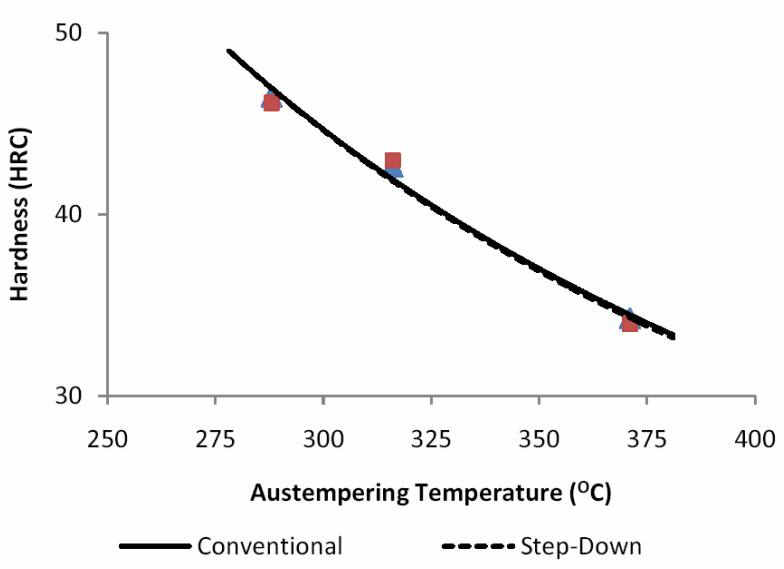

Figure 9. A plot of hardness vs. austempering temperature.

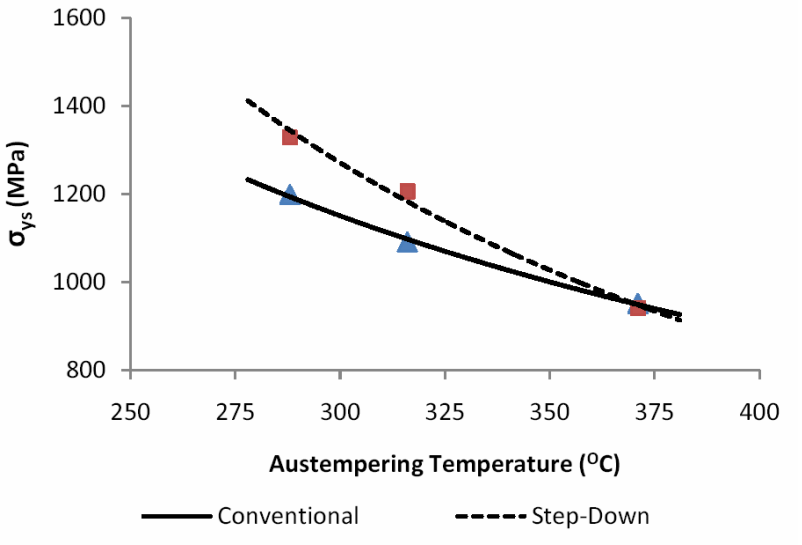

Figure 10. A plot of yield strength vs. austempering temperature.

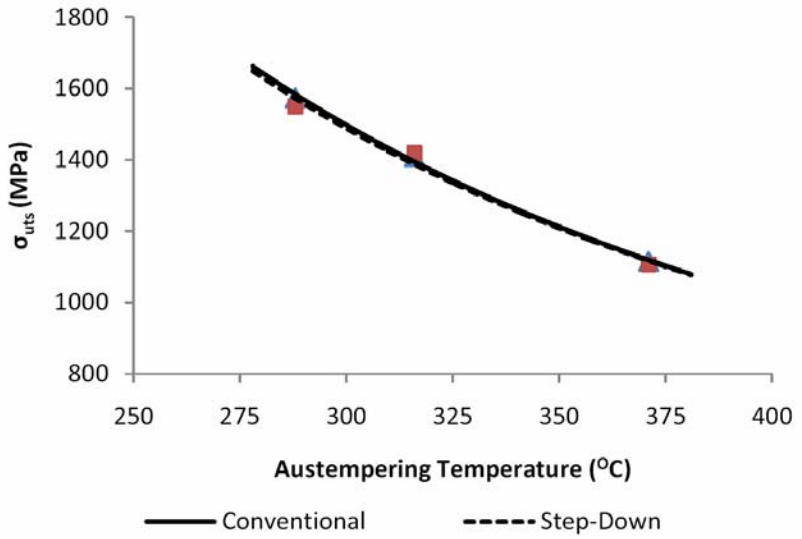

Figure 11. A plot of ultimate strength vs. austempering temperature.

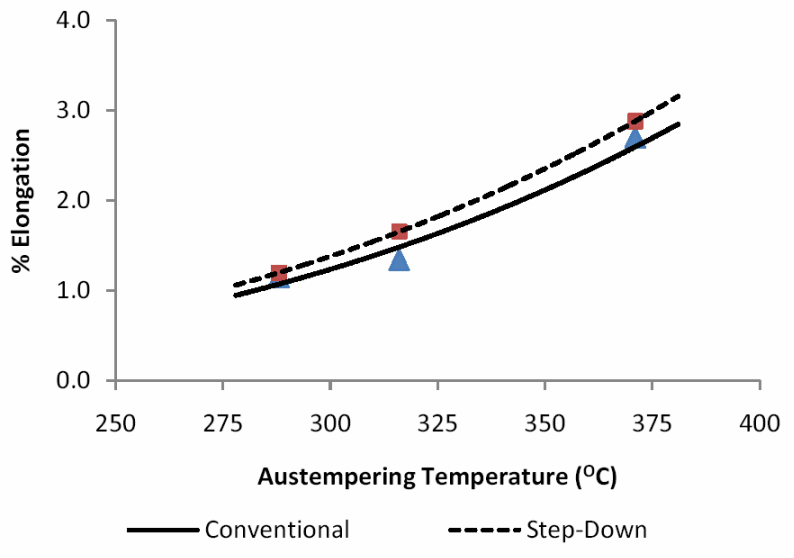

Figure 12. A plot of % elongation vs. austempering temperature.

Figure 13 reports the effect of austempering temperature on the fracture toughness of ADI processed by both step-down and conventional austempering process. It is evident from this figure that the fracture toughness increases as the austempering temperature increases. The present test results also show that, there was no significant difference in the fracture toughness values of step-down and conventionally austempered samples. The reason for increase in fracture toughness at higher temperature has been explained below.

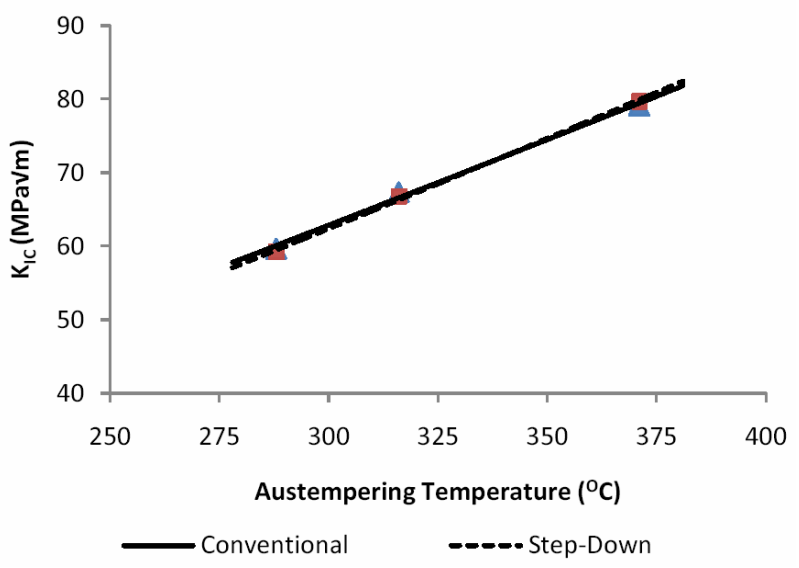

Figure 13. A plot of fracture toughness vs. austempering temperature.

The fracture toughness of ADI will be dependent on both the austenitic carbon content $(X_\gamma.C_\gamma)$ and the ferritic cell size (d) or mean free path of dislocation motion. The higher austenitic carbon $(X_\gamma.C_\gamma)$ will increase the strain hardening rate of austenite and consequently will increase its fracture toughness [23]. The lower mean free path of dislocation (d) will also increase the fracture toughness because, it is well known that the smaller grain size is beneficial for fracture toughness. An analytical model was earlier developed by one of these investigators (SKP) [24], which indicate the fracture toughness will be proportional to the parameter $(X_\gamma.C_\gamma / d)^{1/2}$. Table 4 reports the effect of austempering temperature on this parameter. It is evident that this parameter increases with the increase in austempering temperature. In Figure 14, the fracture has been plotted against this parameter. Obviously, increased fracture toughness is obtained as the parameter $(X_\gamma.C_\gamma / d)^{1/2}$ increases, thus validating our earlier model.

Table 4. Influence of austempering temperature on the parameter $\sqrt{(X_\gamma.C_\gamma / d)}$

Austempering temperature (°C)	$\sqrt{(X_\gamma.C_\gamma / d)}$ (conventional)	$\sqrt{(X_\gamma.C_\gamma / d)}$ (step-down)
288	0.1054	0.1123
316	0.1395	0.1229
371	0.1588	0.1534

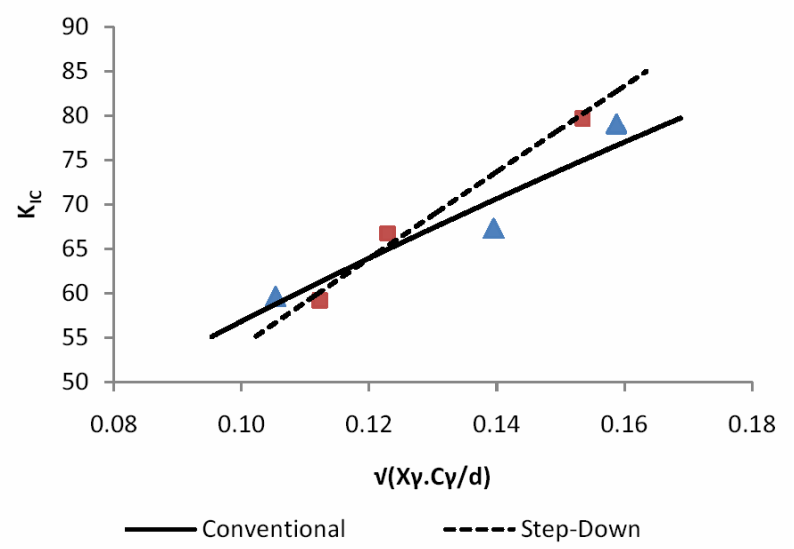

Figure 14. A plot of K_{IC} vs. $\sqrt{(X_\gamma.C_\gamma / d)}$.

In summary, the present test results show that, there is no significant difference in the mechanical properties and fracture toughness of ADI processed by step-down and conventional austempering process. Several investigations [1, 6, 11, 15, 27] in the past have tried step-down austempering process to improve the mechanical properties of ADI. Bayati and Elliot [6] applied a step-down austempering process in a high manganese ductile cast iron in order to prevent formation of martensite in the inter-cellular region. They reported that a mixed microstructure, which consisting of upper bainite near the graphite nodules and lower bainite in the inter-dendritic region obtained by step-down austempering

process and this resulted in better mechanical properties in their samples. Ahmedabadi et al. [1] used a similar step-down austempering process and observed reduction in volume fraction of untransformed austenite in the segregated regions. They reported an increase in impact strength, but no significant difference in either yield or tensile strengths of the materials processed by step-down or conventional austempering process. In the present investigation also, no significant difference in yield and tensile strength of the materials processed by step-down and conventional austempering process was observed even though the process used here is slightly different from above investigators.

Perloma and Anderson [27] used a step-down austempering process similar to Bayati and Elliot, but observed no significant improvement in properties of ADI compared to conventional austempering process. Grech [11] also carried out a step-down austempering process, but observed no significant changes in mechanical properties. The present test results are in agreement with the observations of Pereloma, Anderson and Grech, where no significant improvements in properties were observed by step-down austempering process. This is because no significant change in microstructure was observed in both the processes, which in-turn did not contribute to any alteration of the properties of the material.

The fractographs of the samples processed by conventional and step-down austempering are shown in Figures 15 and 16, respectively. The fractographs show typical mixture of quasi-cleavage and dimples (ductile fracture) and the proportion of ductile fracture increases with the increase in austempering temperature. Again, no significant difference in fracture mode was observed between step-down and conventionally austempered samples at the same austempering temperature.

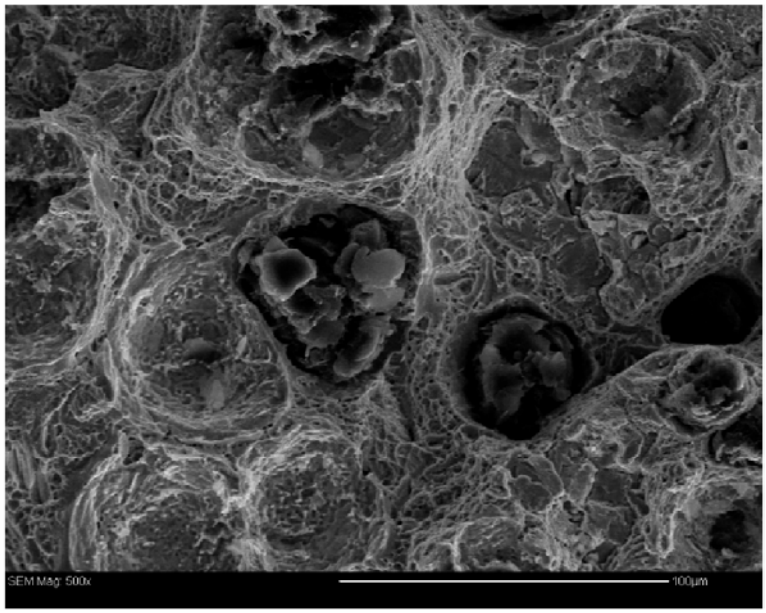

(a)

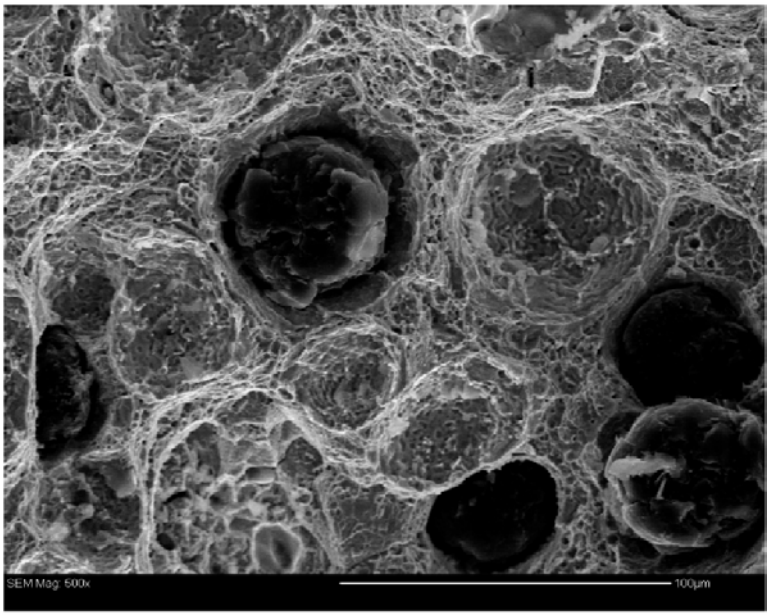

(b)

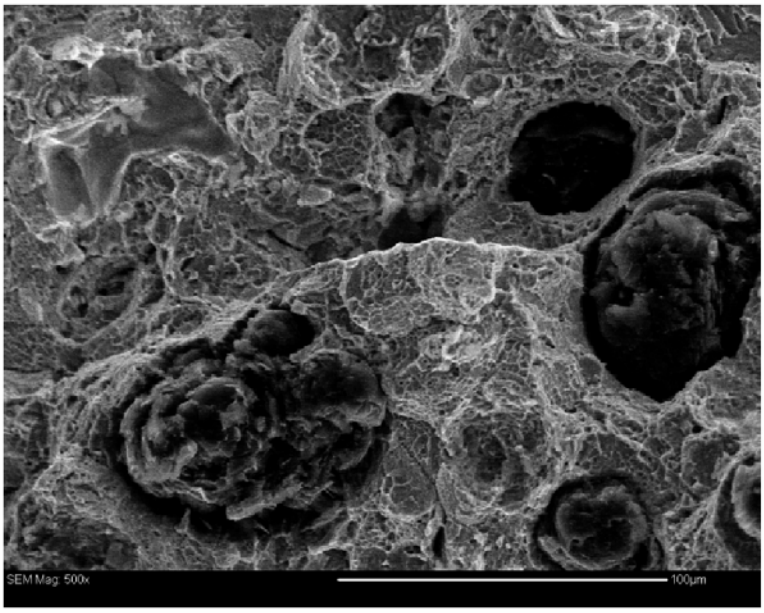

(c)

Figure 15. Fractographs of ADI heat-treated by conventional austempering process produced using SEM at 500X. All samples were austenitized at 927°C (1700°F) for 2h and austempered in salt bath maintained, respectively, at: (a) 288°C (550°F); (b) 316°C (600°F); and (c) 371°C (700°F).

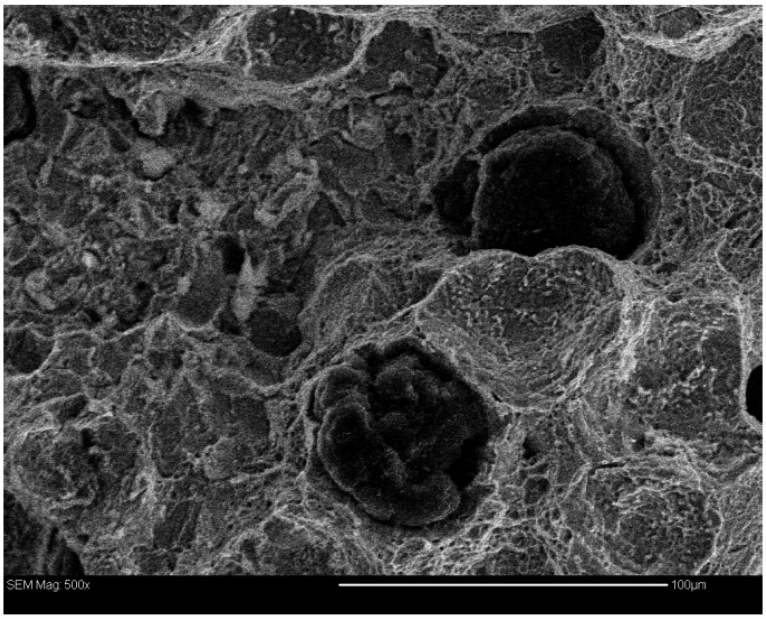

(a)

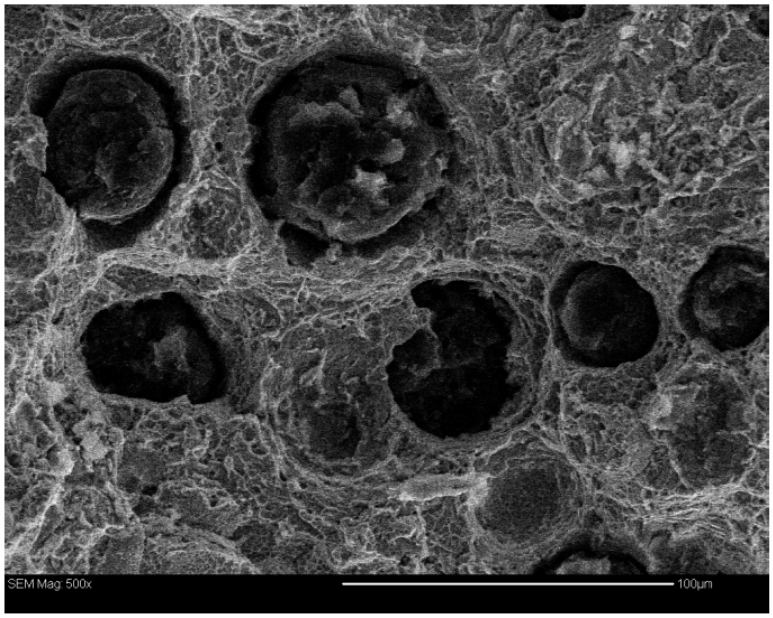

(b)

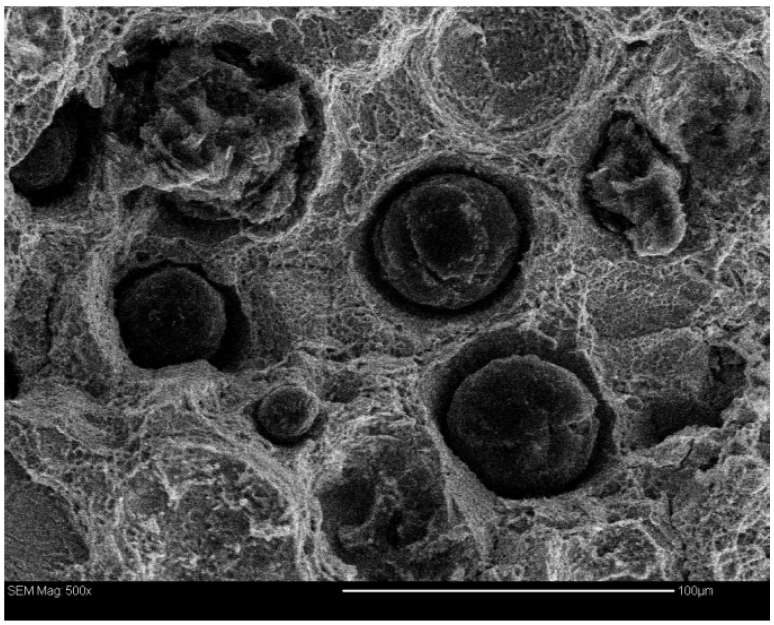

(c)

Figure 16. Fractographs of ADI heat-treated by step-down austempering process produced using SEM at 500X. All samples were austenitized at 927°C (1700°F) for 2h and austempered in salt bath maintained at: (a) 288°C-260°C (550°F-500°F); (b) 316°C-288°C (600°F-550°F); and (c) 371°C-343°C (700°F-650°F).

It must be pointed out that while step-down austempering process used in this investigation did not improve the mechanical properties of unalloyed ductile cast iron, it also did not cause any reduction in any of the mechanical properties including the fracture toughness of the material. Moreover, the step-down austempering process has the added advantage of reduced energy cost since the average temperature of the salt bath is lower than in conventional austempering process. Thus, it appears that this type of step-down austempering can be a viable heat treatment process for ADI without compromising any of the mechanical properties of ADI.

As mentioned earlier, a closer examination of the microstructure also revealed that, there was some untreated austenite left over in the material after the austempering process. The proportion of the unreacted

austenite (γ) was higher in the step-down austempering process. This unreacted austenite (γ) has lower carbon content and because of their blocky appearance, they are nonuniform in carbon content and will transform onto martensite during loading by stress induced martensite formation thereby causing reduction in fracture toughness. It therefore appears that by austempering for a longer period of time while using the step-down austempering process, it may be possible to improve the fracture toughness and other mechanical properties of ADI.

4. Conclusions

(1) Both step-down and conventional austempering process resulted in a very similar microstructure in unalloyed ductile cast iron at same austempering temperatures.

(2) Both the ferrite and austenite coarsens as the austempering temperature increases.

(3) The mechanical properties including fracture toughness of unalloyed ductile cast iron processed by step-down and conventional austempering processes were very similar.

(4) The fracture toughness of ADI increases with the increase in the austempering temperature and the parameter $(X_\gamma.C_\gamma / d)^{1/2}$.

(5) The fracture toughness was higher in the upper bainitic temperature region than in the lower bainitic temperature.

(6) It appears that it is possible to produce ADI at a lower energy cost using the step-down austempering process without compromising any of the mechanical properties.

(7) The present test results also indicate that in step-down austempering process, a longer period of austempering may improve mechanical properties of the ADI.

References

[1] M. N. Ahmadabadi, T. Ohide and E. Niyam, Effects of successive stage austempering on the structure and impact strength of high Mn-ductile iron, Cast Metal 5(2) (1992), 62-72.

[2] ASTM E-8: Standard Test Method for Tensile Testing of Metallic Materials, Annual Book of ASTM Standards, ASTM, 3.01 (1992), 542-566.

[3] ASTM E-399: Standard Test Method for Plane Strain Fracture Toughness Testing of Metallic Materials, Annual Book of ASTM Standard, PA, 3.01 (1992), 745-756.

[4] L. Bartosiewicz, B. V. Kovacs, A. R. Krause and S. K. Putatunda, Fatigue crack growth behaviour of austempered ductile cast iron, AFS Transactions 92 (1992), 135-142.

[5] L. Bartosiewicz, I. Singh, F. A. Alberts, A. R. Krause and S. K. Putatunda, Influence of microstructure on high cycle fatigue behaviour of austempered ductile cast iron, Materials Characterization 30 (1993), 221-234.

[6] H. K. Bayati and R. Elliot, Stepped austempering heat treatment of a 0.67% Mn-Mo-Cu ductile iron, Materials Science and Technology 13 (1998), 117-123.

[7] R. Boschen, H. Bomas, P. Mayr and H. Vetters, Strength and fatigue of austempered ductile iron (ADI), Proceedings of the 2nd International conference on austempered ductile cast iron, Ann Arbor, MI; ASME, Gear Research Institute: Naperville, IL, (1986), 179-185.

[8] B. D. Cullity, Elements of X-ray Diffraction, Addison-Wesley: Reading, MA, 1974.

[9] J. Dodd, High strength, high ductility ductile iron, Modern Casting 68 (1978), 60-66.

[10] J. L. Doong and C. Chen, Fracture toughness of bainitic nodular cast iron, Fatigue and Fracture of Engineering Material Structure 12 (1989), 155-165.

[11] M. Grech, P. Bowen and J. M. Young, Effect of Austempering Temperature on the Fracture Toughness and Tensile Properties on ADI Alloyed with Copper and Nickel, World Conference on ADI, Bloomingdale, Chicago, IL (1991), 328-374.

[12] R. B. Gundlach and J. F. Janowak, Development of ductile iron for commercial austempering, American Foundry Society Transactions 94 (1983), 377-388.

[13] R. B. Gundlach and J. F. Janowak, Austempered ductile irons combine strength with toughness and ductility, Metal Progress 128 (1985), 19-26.

[14] R. A. Harding, Effects of metallurgical process variables on austempered ductile iron, Cast Iron 2 (1986), 65-71.

[15] C. H. Hsu and T. L. Chuang, Influence of stepped austempering process on the fracture toughness of austempered ductile iron, Metallurgical and Materials Transaction A 32 (2001), 2509-2513.

[16] M. Johansson, Austenitic-bainitic ductile iron, American Foundry Society Transaction 85 (1977), 117-122.

[17] B. V. Kovacs, J. R. Keough and D. M. Pramstaller, The Austempered Ductile Iron Process, Final Report to the Gas Research Institute, NTIS No. PB89190946LP, 1989.

[18] B. V. Kovacs and J. R. Keough, Physical properties and application of austempering grey iron, American Foundry Society Transactions 101 (1993), 283-291.

[19] D. J. Moore, T. N. Rouns and K. B. Rundman, The effect of heat treatment, mechanical deformation and alloying elements on the rate of bainitic formation in austempered ductile cast iron, Journal of Heat Treating 41 (1985), 7-24.

[20] D. J. Moore, T. N. Rouns and K. B. Rundman, Structure and mechanical properties of austempered ductile iron, AFS Transactions 93 (1985), 705-718.

[21] T. Nakamura, K. Kishima, K. Jnibo, Y. Matsuo and F. Nugai, Fatigue strength of austempered ductile iron cylinders subjected to repeated internal pressure, Journal of Society of Mechanical Engineers Int. J. A 36 (1993), 348-353.

[22] S. K. Putatunda and I. Singh, Fracture toughness of unalloyed austempered ductile cast iron, Journal of Testing and Evaluation 23(5) (1995), 325-332.

[23] S. K. Putatunda and P. K. Gadicherla, Influence of austenitizing temperature on fracture toughness of a low manganese austempered ductile iron (ADI) with ferritic as cast structure, Materials Science and Engineering A A268 (1999), 15-31.

[24] S. K. Putatunda and P. K. Gadicherla, Effect of austempering time on mechanical properties of a low manganese austempered ductile iron, Journal of Materials Engineering and Performance 9(2) (2000), 193-203.

[25] S. K. Putatunda, Influence of austempering temperature on fracture toughness of a low manganese austempered ductile iron (ADI), Materials and Manufacturing Processes 16(2) (2001), 245-263.

[26] S. K. Putatunda, Comparison of the mechanical properties of austempered ductile cast iron processed by conventional and step-down austempering process, Materials and Manufacturing Process 25(9) (2010).

[27] E. V. Pereloma and C. S. Anderson, Microstructure and properties of austempered ductile iron subjected to single and two-step processing, Materials Science and Technology 22 (2006), 1112-1118.

[28] P. P. Rao and S. K. Putatunda, Influence of microstructure on fracture toughness of austempered ductile cast iron, Metallurgical and Materials Transactions 28A (1997), 1457-1470.

[29] P. P. Rao and S. K. Putatunda, Comparative study of fracture roughness of austempered ductile cast iron with upper and lower ausferritic microstructure, Materials Science and Technology 14 (1998), 1257-1263.

[30] P. P. Rao and S. K. Putatunda, Dependence of fracture toughness of austempered ductile cast iron on austempering temperature, Metallurgical and Materials Transactions 29A (1998), 3005-3016.

[31] P. K. Rastogi, A Comparative Evaluation of Mechanical Properties and Machinability of Austempered Ductile Iron (ADI) and Micro-alloyed Steel, SAE Paper Series, International Congress and Exposition, Detroit, Michigan, 1991.

[32] C. S. Roberts, Effect of carbon on the lattice parameter of austenite, Transactions of AIME 197 (1982), 203-204.

[33] K. B. Rundman and R. C. Klug, X-ray and metallographic studies of an austempered ductile iron, American Foundry Society Transactions 90 (1982), 499-508.

[34] I. Schmidt and A. Schuchert, Unlubricated wear of austempered ductile cast iron, Z Metal Kunde 78 (1987), 871-875.

[35] P. Shanmugam, P. P. Rao, K. R. Udupa and N. Venkataraman, Effect of microstructure on fatigue strength of austempered ductile iron, Journal of Materials Science 29 (1994), 4933-4940.

[36] R. C. Voigt and C. R. Loper, Proceedings of 1st International Conference on Austempered Ductile Iron, Vol. 83, Metals Park, Ohio, 1984.

[37] J. Yang and S. K. Putatunda, Improvement in strength and toughness of austempered ductile cast iron by novel two-step austempering process, Materials and Design 25 (2004), 219-230.

[38] J. Yang and S. K. Putatunda, Near threshold fatigue crack growth behaviour of austempered ductile cast iron (ADI) processed by a novel two-step austempering process, Materials Science and Engineering A A382 (2004), 265-279.

[39] J. Yang and S. K. Putatunda, Effect of microstructure on abrasion wear behaviour of austempered ductile iron processed by a novel two-step austempering process, Materials Science and Engineering A A406 (2005), 217-228.

■